Electronic Supplementary Material (ESI) for Environmental Science: Processes & Impacts.
This journal is © The Royal Society of Chemistry 2022

Torgeson, Rosenfeld, et al., 2022.

Supplementary Information

Title: Hydrobiogechemical interactions in the hyporheic zone of a sulfate-impacted, freshwater stream and riparian wetland ecosystem

Authors: Joshua M. Torgeson[a,#,*], Carla E. Rosenfeld[b,*], Aubrey J. Dunshee[a], Kelly Duhn[c,##], Riley Schmitter[a], Patrick A. O'Hara[a], G.H. Crystal Ng[a,d], Cara M. Santelli[a,c**]

[a]Department of Earth and Environmental Sciences, University of Minnesota, Minneapolis, MN 55455, USA

[b]Section of Minerals and Earth Sciences, Carnegie Museum of Natural History

[c]BioTechnology Institute, University of Minnesota, St. Paul, MN 55108, USA

[d]St. Anthony Falls Laboratory, University of Minnesota, Minneapolis, MN 55455, USA

*Co-first authorship: J.M. Torgeson and C.E. Rosenfeld contributed equally to this manuscript

**Corresponding Author. Tel.: +1 612-624-9760; Fax: +1 612-625-5780; Email: santelli@umn.edu

Present Address:

[#]Pacific Northwest National Laboratory, Richland, Washington 99352, USA

[##]Water Resources Science, University of Minnesota, Duluth, MN

Email addresses: torge158@umn.edu (J.M. Torgeson), rosenfeldc@carnegiemnh.org (C.E. Rosenfeld), duns0034@umn.edu (A. Dunshee), duhnx004@d.umn.edu (K. Duhn), schm4386@umn.edu (R. Schmitter), ohara060@umn.edu (P. O'hara), gcng@umn.edu (G.H.C. Ng), santelli@umn.edu (C.M. Santelli)

TABLE OF CONTENTS

Methods

Iron X-ray absorption spectroscopy (XAS) analysis

For Fe XAS analysis, samples were run as wet pastes by pressing the sediment into a 1x4 cm slit bored into a 1/8" polycarbonate sample holder in an anoxic glovebag. The sediment was capped on both sides with Kapton film (25µm thick) and transported to the beamline in a N_2 purged container. Fe K-edge X-ray absorption near edge structure (XANES) and extended X-ray absorption fine structure (EXAFS) spectra were collected at beamline 10-BM equipped with a Si(111) crystal monochromator and a N_2-purged Lytle detector to avoid sample oxidation and reduce signal scatter. Fluorescence spectra were collected with the Lytle detector positioned 90˚ to the incident beam. For each environmental sample, ~9-16 scans were collected in quick-XAFS mode and successive scans were monitored for white-line shifts or other changes in spectra indicative of beam damage or radiation-induced oxidation. Scans were collected from -250 to +800 eV around the Fe K-edge. Data reduction, normalization, and analysis was performed in the Athena program in Demeter (version 0.9.26)[1]. EXAFS spectra were background subtracted, k^3-weighted, and analyzed from 3-12 $Å^{-1}$.

Linear combination fitting (LCF) analysis was performed on the Fe XANES region over the energy range -20 to +30 eV with single valence Fe reference materials to determine Fe oxidation state. Fe speciation analysis was performed via LCF of k^3-weighted spectra over a k-range of 2-10 $Å^{-1}$ following principal component analysis (PCA) and target transformation analysis (TTA). The potential number of components was determined for the whole dataset via PCA and fitness of reference compounds to the overall dataset were evaluated via TTA. A library of Fe reference compounds was used to identify and quantify structural components in individual samples using linear combination fitting (LCF). In our LCF approach, binding energies were fixed and negative component contributions were prohibited. Goodness of fit was established by minimization of the *R* factor (normalized sum of squares; NSS) parameter. The reference library was made up of powdered Fe(II/III) minerals and organic compounds with well characterized composition and included iron oxide (Fe_2O_3; Baker Chemical), hematite (α-Fe_2O_3; Baker Chemical; synthetic; USGS reflectance standard GDS2[2]), 2-line ferrihydrite (synthetic), nontronite (NG-1; Source Clays Repository), ferric citrate (synthesized[3]), hematite (α-Fe_2O_3; Baker Chemical; synthetic,), lepidocrocite (□-FeO(OH), magnetite (Fe_3O_4; Skyspring Nano 331S Dx), biotite, ferrous chloride ($FeCl_2$; Sigma Aldrich), ferrous sulfate ($FeSO_4$; Sigma Aldrich), vivianite ($Fe_3(PO_4)_2{\cdot}8H_2O$; Priest River, ID), siderite ($FeCO_3$; Roxbury, CT), chalcopyrite ($CuFeS_2$), pyrite (FeS_2), pyrrhotite-4C (Fe_7S_8; Ward Hill, MA, sold by Alpha Aesar), and mackinawite (FeS).

Dr. Brandy Toner provided the raw mackinawite spectrum as well as the previously-characterized mineral specimens of 2-line ferrihydrite, chalcopyrite (A1), sphalerite (S2), pyrite (S7), and nontronite as described previously[4]. Dr. Joshua Feinberg provided the specimens of vivianite, pyrrhotite-4C, goethite (WS222), hematite, lepidocrocite, and magnetite.

Sulfur X-ray Absorption Near Edge Structure (XANES) Analysis

Samples for S XANES were prepared as a wet paste as described above, but only the back of the sample was sealed with Kapton tape and the part of the sample that interacts with the X-rays was left open to avoid trapping N_2 gas that could interfere with the S signal. S-XANES spectra were collected at beamline 9-BM at APS using a Si(111) monochromator. Analysis was performed inside a sealed chamber purged with helium and fluorescence spectra were collected with a 4-element Vortex detector positioned 90˚ to the incident beam. Incident beam energy was calibrated using sodium thiosulfate. XANES spectra were collected from -30 to +240 eV around the S K-edge. Data reduction, normalization, and analysis, including PCA and LCF, was performed in Athena, as described above. The reference library for LCF of the S XANES spectra was made up of powdered S minerals and organic compounds with oxidation states ranging from -2 to +6 and included: mackinawite (FeS), pyrite (FeS_2), elemental sulfur (S_8), sodium thiosulfate (Na_2SO_3), potassium sulfite (K_2SO_3), gypsum ($CaSO_4$), L-cysteine ($C_3H_7NO_2S$), methionine ($C_5H_{11}NO_2S$), DL-methionine sulfoxide ($C_5H_{11}NO_3S$), potassium tetrathionate $(K_2S_4O_6)^{2-}$, sodium dodecyl sulfate (SDS, also known as sodium laurel sulfate; $CH_3(CH_2)_{11}SO_4Na$), sodium polysulfide (Na_2S_4), sulfanilamide ($C_6H_8N_2O_2S$), thiophene (2-thio-phenecarboxylic acid), and amino naphthol sulfonic acid (ANSA). All references were supplied by Dr. Brandy Toner and the preparation and analysis information is described in Cron et al.,(2019)[4]. Linear combination fitting of the sample spectra with the reference spectra was performed using *mrfitty*[5].

Results

Nutrient trends

In the channel, porewater PO_4 concentrations were higher in the summer months (0.38, 0.32, and 0.37 ppm, mean from the peepers for June, July, and August, respectively) than in October (0.06 ppm, mean) with no observable trends with depth into the sediment (Table S1,

Fig. S2). The concentrations measured in the peeper porewaters were similar to those measured from the depth-averaged rhizon concentrations for the 0-10cm and 10-20 cm ranges. Interestingly in both wetland locations, porewater PO_4 concentrations from rhizon samples differed substantially from those collected from peepers, with PO_4 values consistently higher in peeper samples (high spatial resolution, but low temporal resolution) for the depth ranges collected from the spatially-averaged (~10 cm) rhizon samples. In the west wetland, vertical porewater PO_4 concentrations increased in the upper 5-10 cm sediment depth and then remained fairly consistent with increasing depth for all months. PO_4 concentrations in the east wetland were highest in July and August, with peeper concentrations peaking at 4.3-8.0 mg/L around 18.7 cm depth in July and 9 mg/L at 6.2 cm depth in August with concentrations steadily decreasing with depth below those maximum levels.

The range of surface water NO_3^- + NO_2^- concentrations (0.075 - 0.95 ppm) were similar to those in the porewaters (0.01 - 0.76 ppm) collected from peepers (Table S1, Fig. S3). In many instances, concentrations were either below detection or just above detection limits (0.1 mg/L) of the analytical method. Likely because of the very low levels, the concentrations measured from rhizon samples were not distinct from those measured from peeper samples.

Molecular-scale characterization of sediment iron

With Fe K-edge EXAFS, both $FeSO_4$ and $FeCl_2$ were identified as major components in many sediment samples. These compounds were not expected to persist as solids in the sediments due to their high solubility, however their identification in the LCF likely represents adsorbed Fe(II) or the aqueous porewater fraction, as the bulk samples were neither dehydrated nor filtered to remove porewaters. During LCF analysis, using only $FeSO_4$ or $FeCl_2$ resulted in the same total relative percentage of Fe(II), therefore aqueous and adsorbed Fe(II) was assumed to be the sum of these two components. As with the ferrous salts, the $FeCl_3$ chloride reference standard likely represents aqueous and adsorbed Fe(III) due to its high solubility and the hydrated nature of the compound during analysis. For these reasons, fits of $FeCl_3$ will be referred to as “aqueous or adsorbed Fe(III)”. The specific Fe-binding ligands were not determined in this study, but given the high organic matter content of the sediments, the Fe(II) and Fe(III) could be complexed by either organic or inorganic ligands. Previous studies have shown that in organic rich peatlands, organically-complexed Fe(II) and Fe(III) can be present in both oxic and anoxic environments[6].

A phyllosilicate was also present as a major component throughout the sediment profile in both wetlands and in the stream channel. Nontronite (a Fe(III)-dominated dioctahedral phyllosilicate) was the specific phyllosilicate analyzed and used for the fitting and is a common Fe-bearing smectite clay in this northern MN region where Second Creek is located[7, 8]. A small

number of samples had chalcopyrite indicated as a possible fit component. There is a high level of similarity between the reference spectra of pyrite and chalcopyrite, likely due to Fe being bound to S in both mineral structures with little interaction between Fe and copper at the molecular scale. The components have been combined and referred to as "iron disulfide" for LCFs (Fig. 8). Geochemical analysis of sediment acid extractions revealed only trace amounts of copper (data not shown), thus it is likely that pyrite is the predominant metal disulfide phase.

Molecular-scale characterization of sediment sulfur

Many studies have entirely overlooked the presence of S intermediates because of the need for specific analytical techniques to detect and possibly quantify these enigmatic S compounds.[9-14] S XANES is one method that can qualitatively distinguish these compounds in natural samples without major sample alterations.[4, 15] However this approach remains challenging, as several S compounds have similar or non-distinct absorption edges, and S is present in a range of organic and inorganic species with mixed valences in the natural environment. For example, elemental S can exist as numerous different allotropes that are non-distinguishable in S XANES.[16] Inorganic polysulfides (S_x^{2-}; x≥2), which were detected in many of our samples, are composed of S chains with one S atom having an oxidation state of -2 and the other S atoms in zerovalent state. The electronic oxidation states, and thus the S K-edge XANES absorption edges, of elemental S and polysulfide are therefore similar, both showing absorption edges at ~2743 eV (Fig. S6). However, in our analysis, the additional inorganic polysulfide absorption peak at lower energies (~2741 eV for our reference NaS_4) resulting from the reduced S^{2-} enables relatively good distinction between the two compounds. This provides confidence that both elemental S and inorganic polysulfides are present in the hyporheic zone of Second Creek.

Contributing even more complexity to the S XANES analysis, the reduced S atom(s) in organic polysulfides (RS_xR') are expected to be shifted toward higher energies than in inorganic (anionic) polysulfides due to presence of the S-C bond. For example, the valence state of S in bisulfide (HS^-) is -1, while in cysteine (HS-R, the organic analog to bisulfide) it is 0.2.[15] Additionally, the spectra of long-chain organic polysulfides would become dominated by S-S bonds, essentially resembling a S(0) spectrum. The resulting effect is that the S XANES spectra of some organic polysulfides have absorption energies and peak features that are overlapping with, and potentially indistinguishable from, that of elemental S.[13]

Tables

Table S1

Geochemistry data[17] is also publicly available at the Environmental Data Initiative (EDI) data portal: DOI:10.6073/pasta/2a03c810518255ce147cccb10e92ace5.

Table S2

Linear combination fit (LCF) results for Fe K-edge XANES analysis. Sample intervals 'top', 'middle', and 'bottom' refer to sediment depth intervals of ~4cm, ~10cm, and ~20cm respectively, in relation to the depth below the sediment-water interface.

		West Wetland				Channel				East Wetland			
		Fe(II)	Fe(III)	Avg Fe Oxidation State	NSS	Fe(II)	Fe(III)	Avg Fe Oxidation State	NSS	Fe(II)	Fe(III)	Avg Fe Oxidation State	NSS
June	top	74	26	2.27	0.0008	57	43	2.43	0.0013	70	30	2.30	0.0017
	middle	53	47	2.47	0.0005	45	56	2.57	0.0062	49	52	2.52	0.0017
	bottom	61	39	2.39	0.0006	33	67	2.67	0.0003	47	53	2.53	0.0021
July	top	55	44	2.44	0.0005	69	30	2.30	0.0003	77	24	2.24	0.0003
	middle					61	39	2.40	0.0003	51	49	2.49	0.0002
	bottom	47	53	2.53	0.0003	64	36	2.36	0.0002				
August	top	73	27	2.28	0.0021	58	43	2.43	0.0025	85	16	2.16	0.0024
	middle	58	42	2.42	0.0005	69	31	2.31	0.0005				
	bottom	47	53	2.54	0.0003	72	28	2.29	0.0018	51	50	2.50	0.0029
October	top	86	14	2.14	0.0004	70	30	2.30	0.0003	56	44	2.44	0.0001
	middle	76	24	2.24	0.0003	53	47	2.47	0.0002	52	48	2.48	0.0002
	bottom	68	32	2.32	0.0004	74	26	2.27	0.0002	47	53	2.53	0.0002

NSS = Normalized sum of squares ($100\sum_i(data_i\text{-}fit_i)^2/\sum_i data^2$).

Table S3

LCF fit results for S k-edge XANES samples. Sample intervals ‘top’, ‘middle’, and ‘bottom’ refer to sediment depth intervals of ~4cm, ~10cm, and ~20cm respectively, in relation to the depth below the sediment-water interface. LCF results are expressed as relative percent for S-containing components in bulk sediment samples with the sum of all S species normalized to 100%. Oxidation indices for each reference compound are listed below the reference name and were obtained from Cron et al., 2019 except where noted[10]. General categories for reference compounds are also noted below each reference name.

	Month	Depth Interval	NSS	Residual (%)	Gypsum	SDS	Sulfanilamide	ANSA	Methionine Sulfoxide	Thiophene	Polysulfide	Elemental S	Tetrathionate	Thiosulfate	Cystine	Pyrite	Mackinawite
					+6.0	+6.0	+5.3	+5.0	+2.0	+1.0	-1.3/-0.1	0	-0.1/+3.3	-1/+5*	-0.4	-1.0	-2
					inorganic oxidized	organic oxidized	organic oxidized	organic oxidized	organic intermediate	organic intermediate	inorganic intermediate	inorganic intermediate	inorganic intermediate	inorganic intermediate	organic reduced	inorganic reduced	inorganic reduced
Channel	June	top	0.00539	4.652	0	0	0	9.443	0	0	49.148	0	0	0	12.884	0	29.614
		middle	0.00606	7.26	0	0	0	31.87	0	29.25	0	26	0	0	0	0	11.58
		bottom	0.04134	18.4	0	0	0	16.886	0	23.894	49.349	14.449	0	0	0	0	0
	August	top	0.00471	5.549	7.614	0	0	0	0	0	0	53.174	0	20.79	0	0	19.564
		middle	0.00134	2.96	0	5.99	0	0	0	0	16.64	64.81	12.07	0	0	0	0
		bottom	0.0012	3.094	0	0	0	7.203	0	13.301	0	47.447	0	0	0	30.744	0
	October	top	0.00387	4.219	0	0	0	6.472	0	0	42.312	22.579	0	0	0	0	30.419
		bottom	0.00342	3.903	5.007	0	0	13.043	0	0	41.74	0	0	0	39.651	0	0
East Wetland	June	top	0.01021	5.545	0	0	0	0	0	0	25.097	0	0	28.254	0	0	48.283
		middle	0.00176	3.73	15.205	0	0	14.18	0	45.724	0	24.907	0	0	0	0	0
		bottom	0.00489	6.214	39.406	0	0	25.29	0	16.868	0	18.355	0	0	0	0	0
	August	top	0.00202	3.5	0	0	0	0	0	0	0	66.34	0	20.45	0	0	13.28
		bottom	0.00349	5.073	0	0	0	15.563	0	15.676	26.166	40.692	0	0	0	0	0
	October	top	0.00281	4.196	8.302	0	8.986	0	0	0	0	62.607	0	0	0	0	20.663
		middle	0.00258	4.451	0	0	0	32.984	8.039	28.482	0	30.53	0	0	0	0	0
		bottom	0.00217	3.516	0	8.775	0	0	0	0	0	31.233	0	21	0	37.218	0
West Wetland	June	top	0.00215	3.617	0	0	0	7.189	0	0	32.442	42.897	0	0	0	0	18.668
		middle	0.00237	3.861	0	0	0	8.213	0	0	0	55.591	0	17.765	0	0	18.591
		bottom	0.00153	2.835	0	0	0	7.301	0	13.917	33.633	44.053	0	0	0	0	0
	August	top	0.00384	4.006	5.745	0	0	11.685	0	0	39.752	42.053	0	0	0	0	0
		middle	0.0015	3.451	6.301	0	0	14.277	0	43.696	0	35.116	0	0	0	0	0
	October	top	0.0036	3.81	0	0	8.681	0	0	0	42.206	24.866	0	0	0	0	25.587
		bottom	0.00196	3.752	0	0	0	11.667	0	18.18	0	0	0	0	0	54.496	15.746

* Oxidation index for thiosulfate obtained from Vairavamurthy et al., 1993

Figures

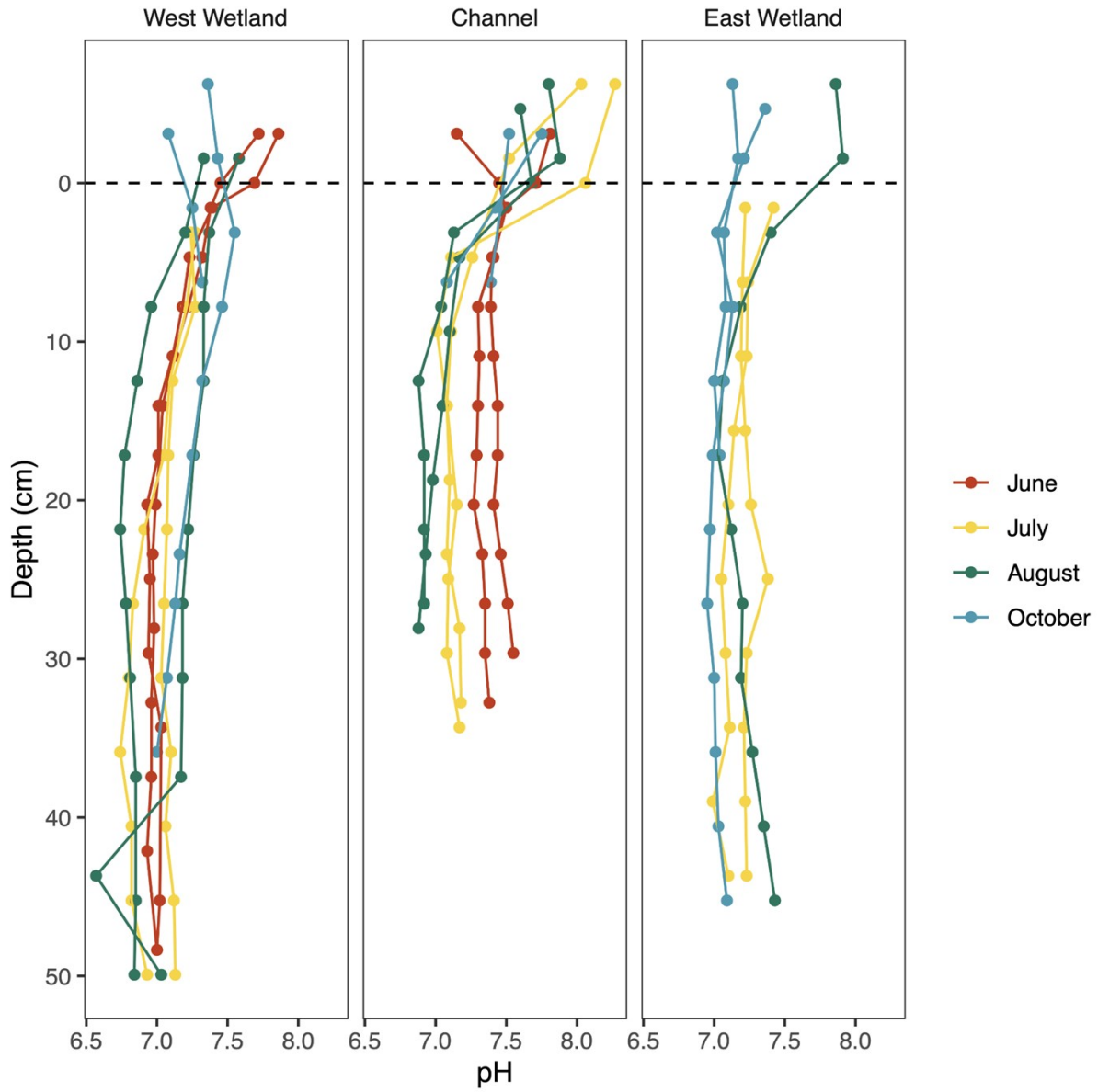

Fig. S1

Measured pH of surface waters and porewaters with depth (cm) at Second Creek in the stream channel and both wetlands collected from replicate peepers during June (red), July (yellow), August (green), and October (blue), 2017. Zero depth (indicated by the black dashed line) marks the sediment-water interface with increasingly positive depth values indicating deeper sediment depth and negative values indicating surface water. Peepers were not installed at any location in May or in the east wetland in June.

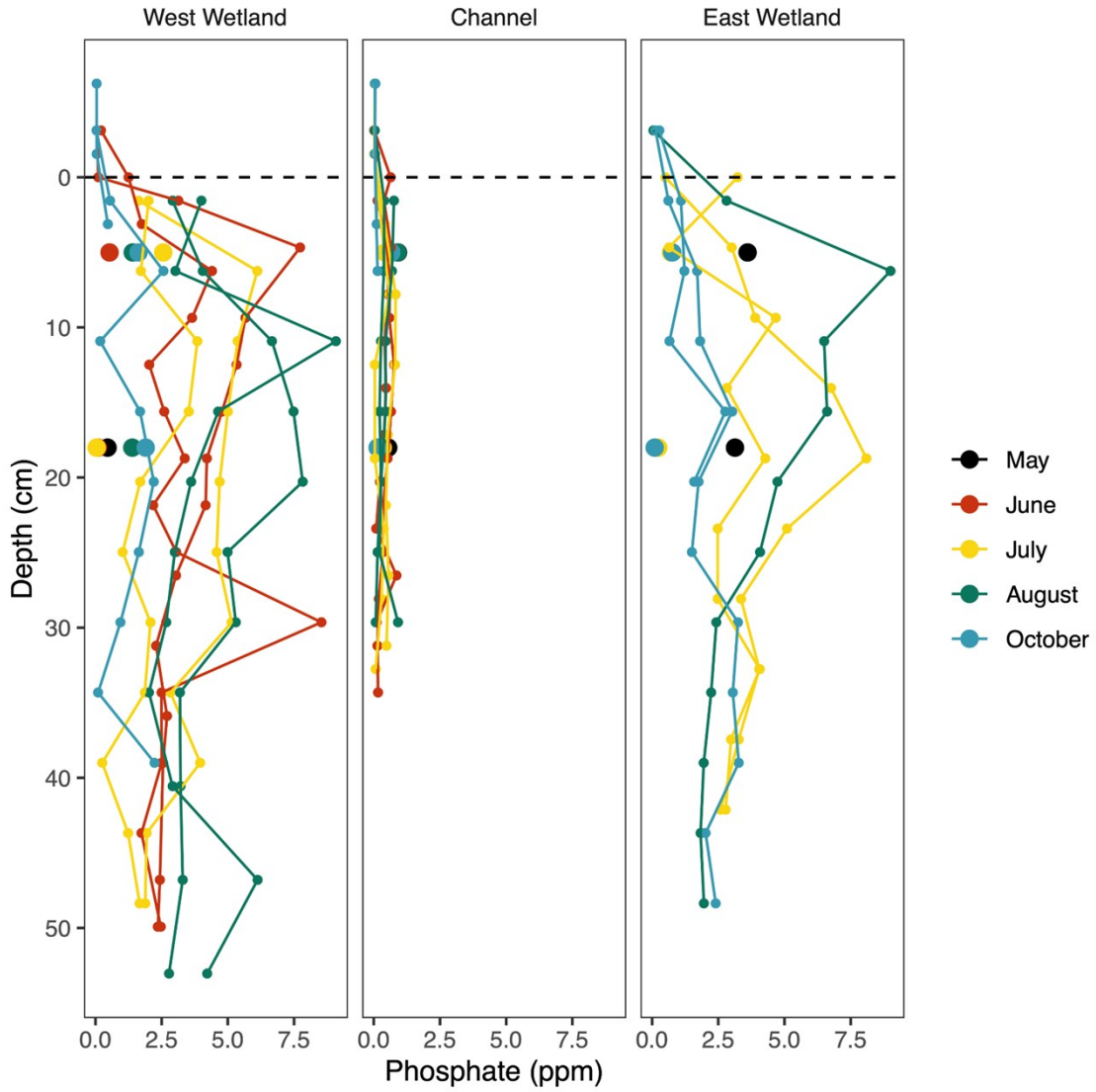

Fig. S2

Dissolved phosphate concentrations of the surface water and porewaters with depth into the sediment in the stream channel and both wetlands collected from replicate peepers and from rhizon samplers during June (red), July (yellow), August (green), and October (blue), 2017. Peeper-collected samples are indicated by small circles connected with lines and rhizon samples are indicated by large circles and represent averaged concentrations from 0-10 cm and 10-20 cm sediment depth. Zero depth (indicated by the black dashed line) marks the sediment-water interface with increasingly positive depth values indicating deeper sediment depth and negative values indicating surface water. Peepers were not installed in any location in May or in the east wetland in June.

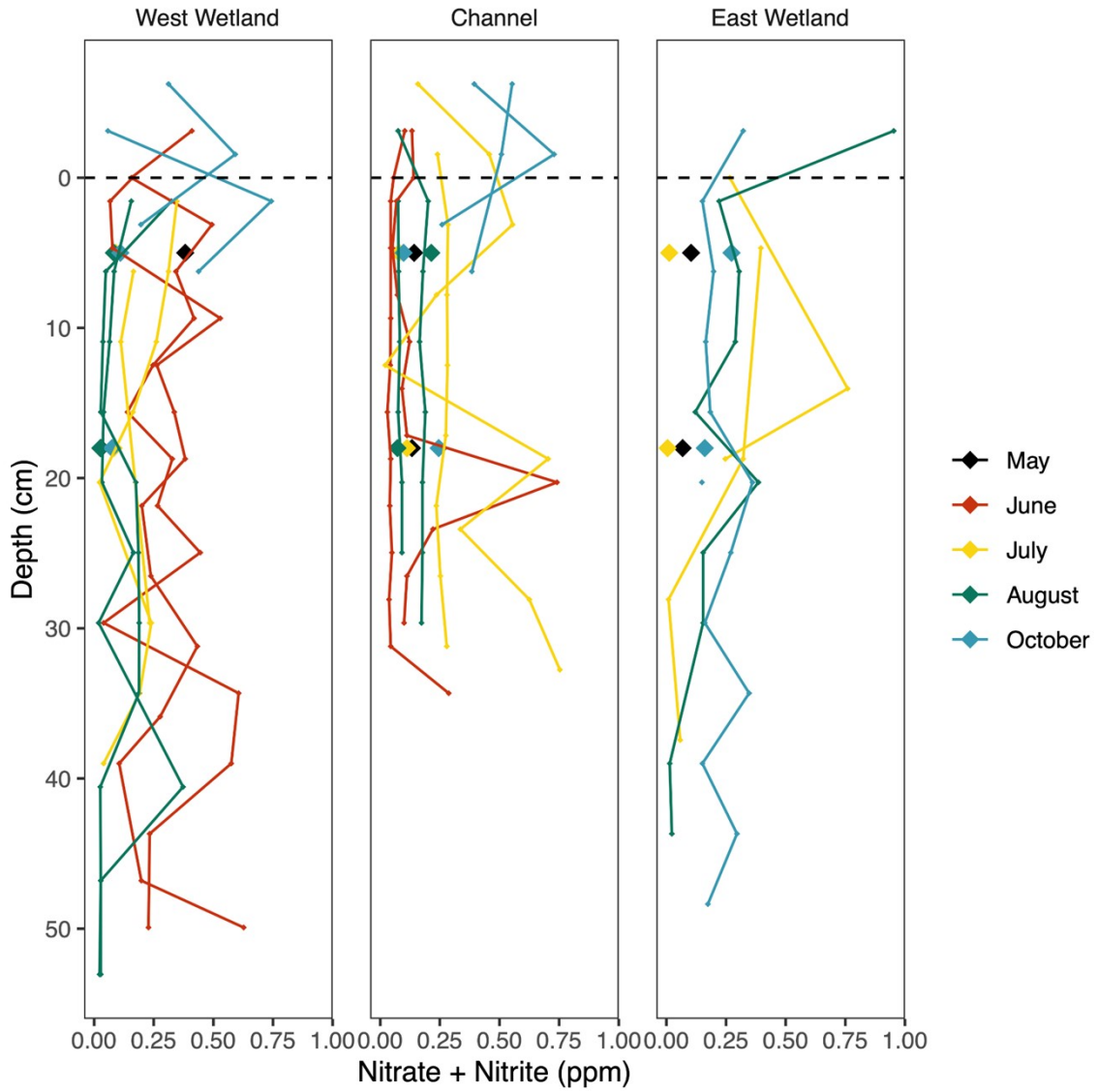

Fig. S3

Dissolved nitrate (NO_3^-) + nitrite (NO_2^-) concentrations of the surface water and porewaters with sediment depth in the stream channel and both wetlands collected from replicate peepers during June (red), July (yellow), August (green), and October (blue), 2017. Peeper-collected samples are indicated by small circles connected with lines and rhizon samples are indicated by large circles and represent averaged concentrations from 0-10 cm and 10-20 cm sediment depth. Zero depth (indicated by the black dashed line) marks the sediment-water interface with increasingly positive depth values indicating deeper sediment depth and negative values indicating surface water. Peepers were not installed at any location in May or in the east wetland in June.

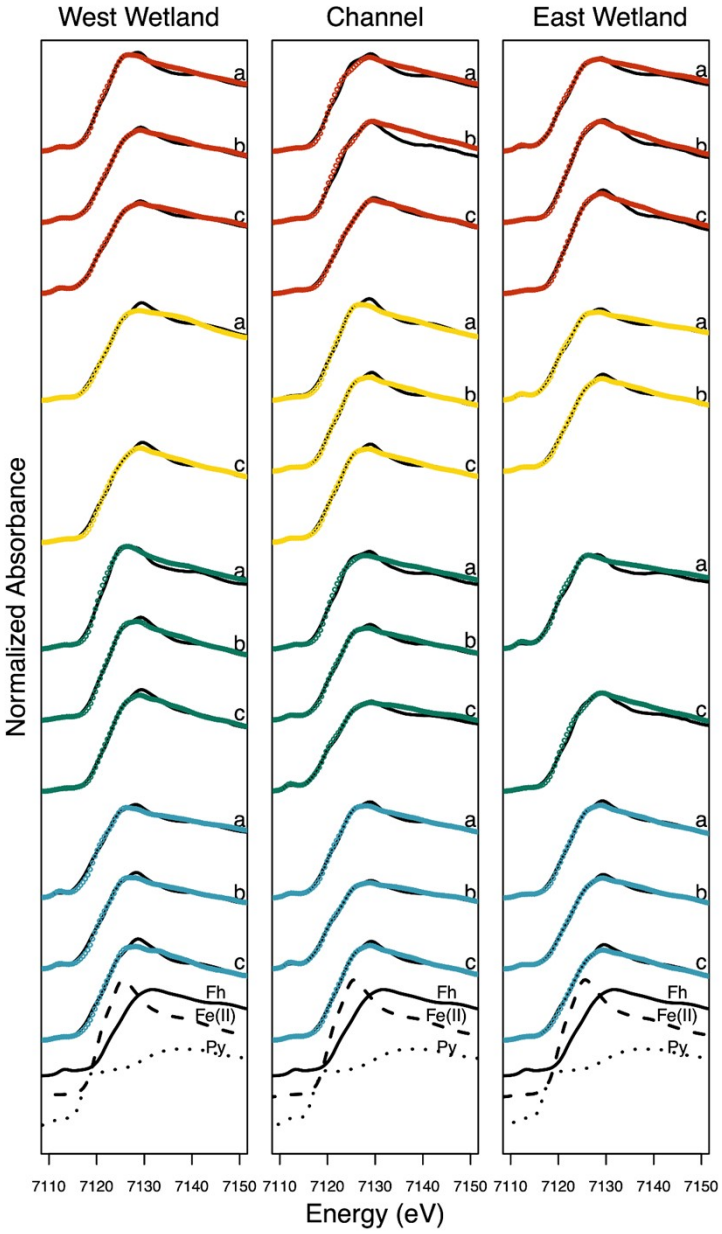

Fig. S4

Normalized Fe K-edge XANES spectra of representative single valence reference materials, sediment samples (solid black lines), and their LCFs (dotted lines) collected in June (red), July (yellow), August (green), and October (blue). Fit results are reported in Table S2. The 'a', 'b', and 'c' denotations refer to the top (~4cm), middle (~10cm), and bottom (~20cm) sediment sampling intervals. Abbreviations for reference spectra: Fh = ferrihydrite, Fe(III) = Fe(III) citrate, Py = pyrite.

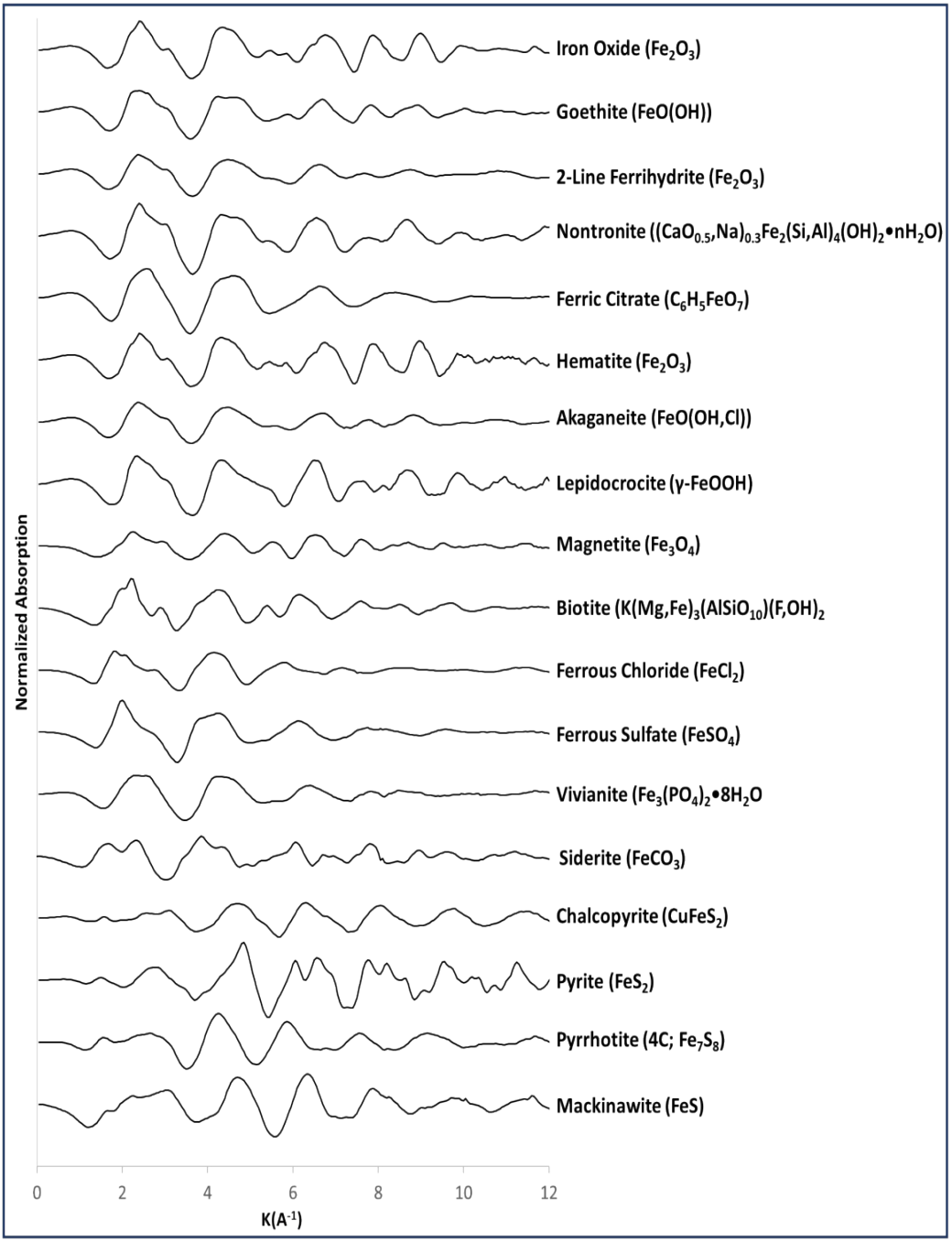

Fig. S5

Normalized Fe K-edge EXAFS spectra of reference standards used to perform linear combination fits. Raw XANES spectra of mackinawite (FeS) courtesy of Dr. Brandy Toner[4].

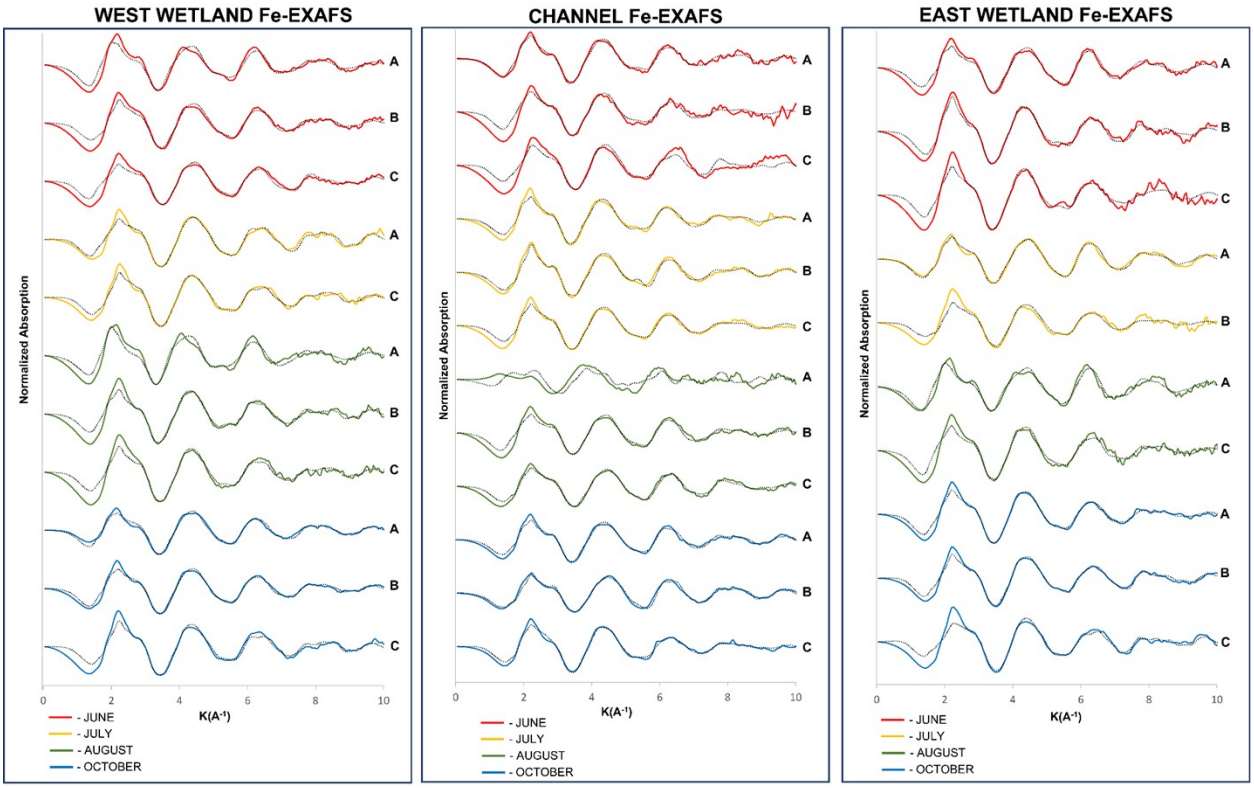

Fig. S6

Experimental k^3-weighted Fe K-edge EXAFS spectra from sediments collected from the west wetland, channel, and east wetland at Second Creek. Experimental spectra are from samples collected in June (red), July (yellow), August (green), and October (blue) with linear combination fits (black dotted line). The 'A', 'B', and 'C' denotations refer to the top (~4cm), middle (~10cm), and bottom (~20cm) sediment sampling intervals.

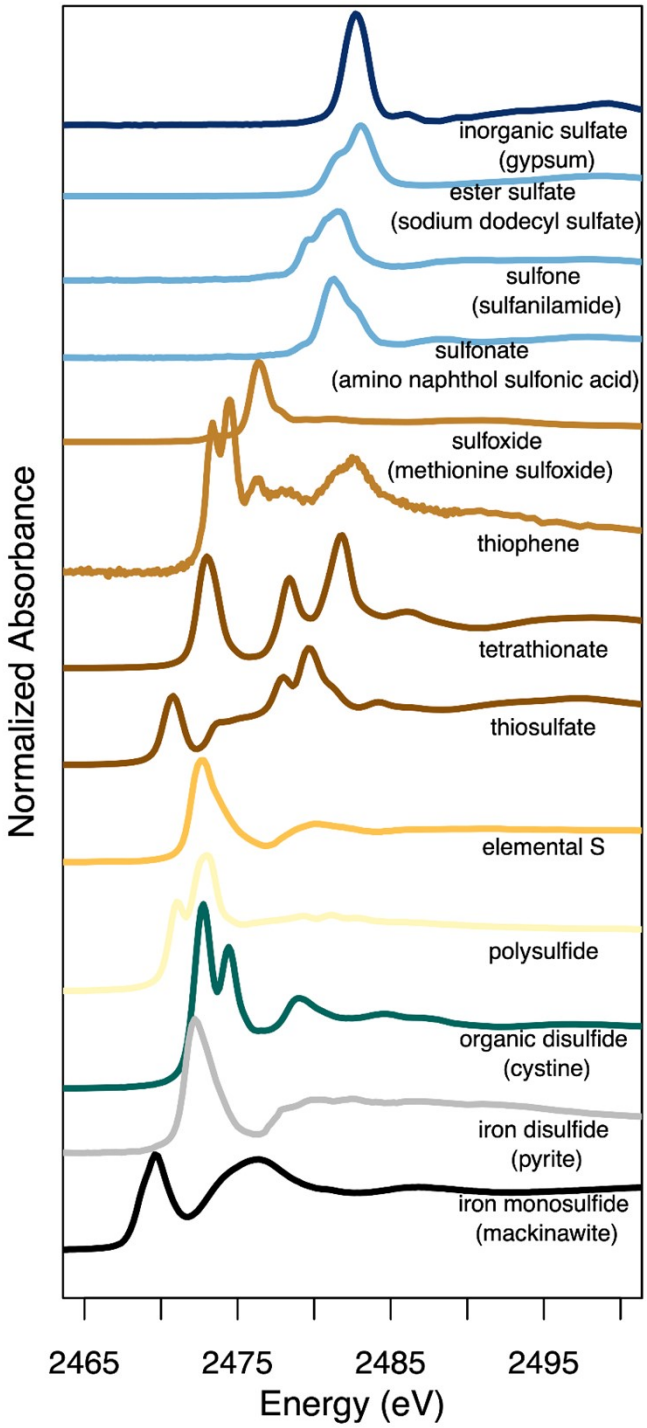

Fig. S7

Normalized S K-edge XANES spectra of reference standards used to perform linear combination fits. Raw XANES spectra courtesy of Dr. Brandy Toner[4].

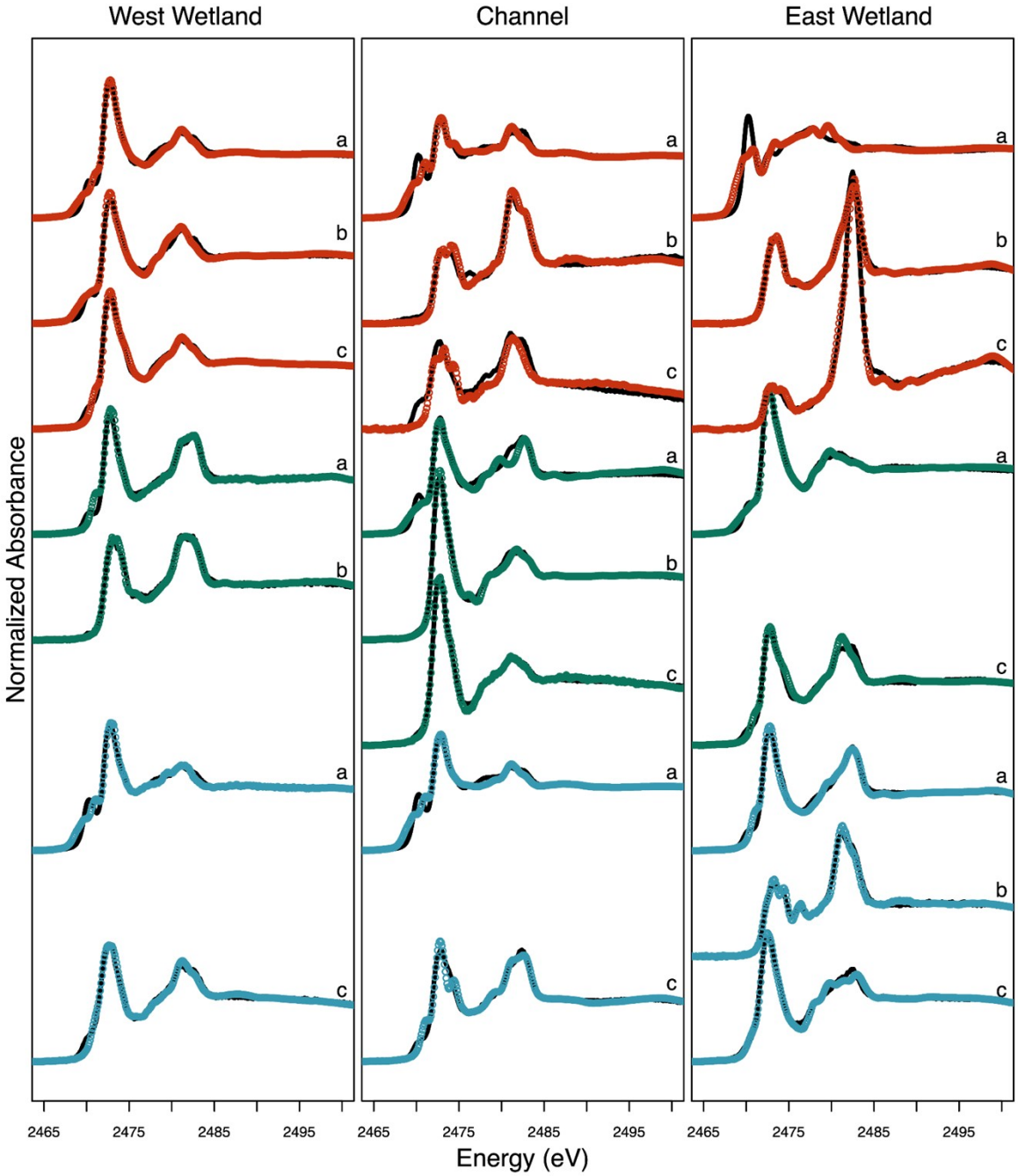

Fig. S8

Experimental S K-edge XANES spectra from sediments collected from the west wetland, channel, and east wetland at Second Creek. Experimental spectra from samples are black lines and linear combination fits are red (June), green (August), and blue (October) dotted lines. The 'a', 'b', and 'c' denotations refer to the top (~4cm), middle (~10cm), and bottom (~20cm) sediment sampling intervals.

References

1. B. Ravel and M. Newville, ATHENA, ARTEMIS, HEPHAESTUS: data analysis for X-ray absorption spectroscopy using IFEFFIT, *J Synchrotron Radiat*, 2005, **12**, 537-541.
2. R. L. Blake, Iron phyllosilicates of the cuyuna district in Minnesota, *Am. Mineral.*, 1965, **50**, 148-169.
3. E. E. Daugherty, B. Gilbert, P. S. Nico and T. Borch, Complexation and Redox Buffering of Iron(II) by Dissolved Organic Matter, *Environ Sci Technol*, 2017, **51**, 11096-11104.
4. B. R. Cron, C. S. Sheik, F.-C. A. Kafantaris, G. K. Druschel, J. S. Seewald, C. R. German, G. J. Dick, J. A. Breier and B. M. Toner, Dynamic Biogeochemistry of the Particulate Sulfur Pool in a Buoyant Deep-Sea Hydrothermal Plume, *ACS Earth and Space Chemistry*, 2019, **4**, 168-182.
5. S. L. Nicholas, M. L. Erickson, L. G. Woodruff, A. R. Knaeble, M. A. Marcus, J. K. Lynch and B. M. Toner, Solid-phase arsenic speciation in aquifer sediments: A micro-X-ray absorption spectroscopy approach for quantifying trace-level speciation, *Geochim. Cosmochim. Acta*, 2017, **211**, 228-255.
6. A. Bhattacharyya, M. P. Schmidt, E. Stavitski and C. E. Martínez, Iron speciation in peats: Chemical and spectroscopic evidence for the co-occurrence of ferric and ferrous iron in organic complexes and mineral precipitates, *Organic Geochemistry*, 2018, **115**, 124-137.
7. J. W. Gruner, Mineralogy and geology of the Mesabi Range, *Iron Range Resources and Rehabilitation Commission, St. Paul, Minn*, 1946.
8. V. L. Ayres, Mineral notes from the Michigan iron country, *Am. Mineral.*, 1940, **25**, 432-434.
9. M. Taillefert, A. B. Bono and G. W. Luther, Reactivity of Freshly Formed Fe(III) in Synthetic Solutions and (Pore)Waters: Voltammetric Evidence of an Aging Process, *Environmental Science & Technology*, 2000, **34**, 2169-2177.
10. M. Taillefert, V. C. Hover, T. F. Rozan, S. M. Theberge and G. W. Luther, The influence of sulfides on soluble organic-Fe(III) in anoxic sediment porewaters, *Estuaries*, 2002, **25**, 1088-1096.
11. M. Wan, A. Shchukarev, R. Lohmayer, B. Planer-Friedrich and S. Peiffer, Occurrence of surface polysulfides during the interaction between ferric (hydr)oxides and aqueous sulfide, *Environ Sci Technol*, 2014, **48**, 5076-5084.
12. D. Solomon, J. Lehmann, K. K. de Zarruk, J. Dathe, J. Kinyangi, B. Liang and S. Machado, Speciation and long- and short-term molecular-level dynamics of soil organic sulfur studied by X-ray absorption near-edge structure spectroscopy, *J Environ Qual*, 2011, **40**, 704-718.
13. M. A. Vairavamurthy, D. Maletic, S. Wang, B. Manowitz, T. Eglinton and T. Lyons, Characterization of Sulfur-Containing Functional Groups in Sedimentary Humic Substances by X-ray Absorption Near-Edge Structure Spectroscopy, *Energy & Fuels*, 1997, **11**, 546-553.
14. T. F. Rozan and G. W. Luther, in *Environmental Electrochemistry*, 2002, DOI: 10.1021/bk-2002-0811.ch019, pp. 371-387.
15. T. Zeng, W. A. Arnold and B. M. Toner, Microscale characterization of sulfur speciation in lake sediments, *Environ Sci Technol*, 2013, **47**, 1287-1296.
16. C. Nims, B. Cron, M. Wetherington, J. Macalady and J. Cosmidis, Low frequency Raman Spectroscopy for micron-scale and in vivo characterization of elemental sulfur in microbial samples, *Sci Rep*, 2019, **9**, 7971.

17. C. E. Rosenfeld, J. M. Torgeson, A. J. Dunshee, K. D. Duhn, R. Schmitter, P. A. O'Hara, G. C. Ng and C. M. Santelli, Summer 2017 porewater and sediment geochemistry data at Second Creek, a sulfate-impacted riparian wetland in northeast Minnesota.*Journal*, 2022, **vers. 1**.